NANO LETTERS

Letter

pubs.acs.org/NanoLett

Single-Walled Carbon Nanotubes: Mimics of Biological Ion Channels

Hasti Amiri,[†] Kenneth L. Shepard,[*,‡] Colin Nuckolls,[*,†] and Raúl Hernández Sánchez[*,†]

[†]Department of Chemistry and [‡]Department of Electrical Engineering, Columbia University, New York, New York 10027, United States

Supporting Information

ABSTRACT: Here we report on the ion conductance through individual, small diameter single-walled carbon nanotubes. We find that they are mimics of ion channels found in natural systems. We explore the factors governing the ion selectivity and permeation through single-walled carbon nanotubes by considering an electrostatic mechanism built around a simplified version of the Gouy−Chapman theory. We find that the single-walled carbon nanotubes preferentially transported cations and that the cation permeability is size-dependent. The ionic conductance increases as the absolute hydration enthalpy decreases for monovalent cations with similar solid-state radii, hydrated radii, and bulk mobility. Charge screening experiments using either the addition of cationic or anionic polymers, divalent metal cations, or changes in pH reveal the enormous impact of the negatively charged carboxylates at the entrance of the single-walled carbon nanotubes. These observations were modeled in the low-to-medium concentration range (0.1−2.0 M) by an electrostatic mechanism that mimics the behavior observed in many biological ion channel-forming proteins. Moreover, multi-ion conduction in the high concentration range (>2.0 M) further reinforces the similarity between single-walled carbon nanotubes and protein ion channels.

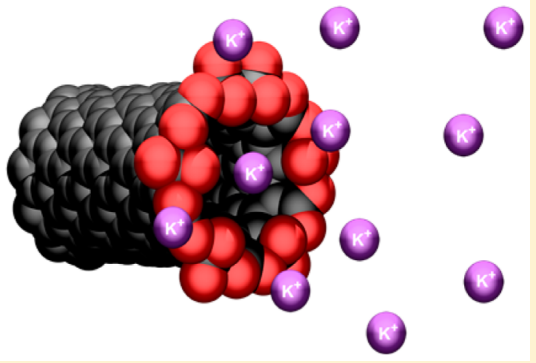

KEYWORDS: *Ion channel, single-walled carbon nanotubes, multi-ion conduction, nanofluidic device*

We demonstrate in this study that ionic conduction through single-walled carbon nanotubes (SWCNTs) is directly analogous to many biological, ion-selective channels. Ion-channels formed from proteins are found in the cellular membranes of all living systems. Understanding their diverse and central roles is important for a deeper understanding of cellular sensing, signaling, and energetics.[1] Ion channels are important targets for drug discovery,[2] and ion channel malfunctions can result in some of the most challenging disorders, including diabetes, epilepsy, cystic fibrosis, cardiac dysrhythmia, and ataxia.[3,4] Artificial nanochannels spanning thin dielectric membranes have been designed to mimic the ion[5−8] and voltage[9] responsivity commonly observed in protein ion channels and to deepen the understanding of the relationship between structure and function of ion channels. Important technological applications have emerged from these efforts including nucleic acid analysis and DNA sequencing through solid-state nanopores.[10] There are significant challenges in fabricating these artificial pores due to variability in the size and characteristics of the pores.[11,12] SWCNTs provide atomically precise and smooth nanochannels with superior chemical and mechanical stability. Small diameter SWCNTs are structurally analogous to transmembrane pore-forming proteins due to their nanometer-sized diameter, hydrophobic core, and ultrafast rate of water transport.[13−15] Moreover, SWCNTs have both adjustable dimensions and tunable surface chemistry.[16] Recently, the transport of both electrolyte and DNA molecules through individual small diameter CNTs have been successfully measured using standard electrophysiological techniques.[17,18]

Figure 1a,b compares the structure of a segment of a (10,0) SWCNT to the structure of the large-conductance Ca^{2+}-activated K^+ channel (CaK) found in nature.[19,20] The similarity in the electrostatic map of each of these pores is striking given the disparity in their building blocks; each pore has a constellation of negative charges on the openings of the channel.[20,21] In the biological system, these fixed charges are responsible for the type and charge of the permeating ions, in addition to gating the pore's conductance.[22,23] To study the ionic transport in SWCNTs, we constructed nanofluidic devices on a silicon wafer that consist of two fluidic reservoirs, patterned in a poly(methyl methacrylate) (PMMA) resist, and connected solely through the interior of only one SWCNT (shown schematically in Figure 1c).[17] We study the ionic conductivity through the SWCNTs by changing the ionic strength, the ion composition, and the pH of the electrolyte solution,[24] and find that the SWCNTs have the same mechanism for conduction as many biological channels. These fixed charges increase the channel conductance by increasing the local concentration and availability of permeating ions at the channel entrance. The ion selectivity and permeation of the SWCNTs can be modeled using a simplified

Received: November 29, 2016
Revised: January 6, 2017
Published: January 19, 2017

DOI: 10.1021/acs.nanolett.6b04967
Nano Lett. 2017, 17, 1204−1211

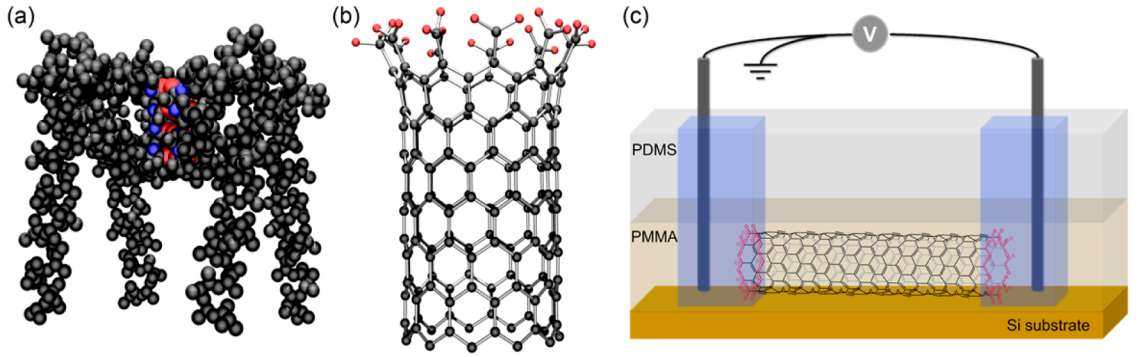

Figure 1. Ion-selective single-walled carbon nanotube-based biomimetic devices. Structural comparison of (a) a biological ion channel with (b) a small-diameter single-walled carbon nanotube. The ionic conductance through both nanochannels is strongly affected by the presence of fixed charges and/or electronegative groups on the pore through an electrostatic mechanism. (a) Side view of the potassium channel MthK (PDB ID: 1LNQ).[19] A ring of eight negative charges is formed at the entrance of the intracellular vestibule of CaK channels, which increases the local concentration of K^+.[20] (b) Model representation of a (10,0) carbon nanotube with a ring of carboxyl groups (oxygen atoms shown in red) present at the channel entrance. The residues along the K-channel and the entrance of the SWCNT are colored for a better view. (c) Schematic of the SWCNT devices studied here. Ionic current−voltage measurements were performed across the two fluidic reservoirs patterned in a PMMA resist through two Ag/AgCl electrodes. The two fluidic reservoirs are connected through the interior of one carbon nanotube (1.5 ± 0.4 nm on average diameter and 20 μm in length) laying on the surface of the Si/SiO_2 substrate. Images are not drawn to scale.

Guoy−Chapman theory that has been successfully applied to many biological channels. Multi-ion conduction in the high concentration range further reinforces the similarity between SWCNTs and protein ion channels due to the single-file transport of ions through the interior of the SWCNTs.

Results and Discussion. *Single-Nanotube Electrophysiological Measurement Platform.* Figure S1 contains a schematic of the device, micrographs of a typical nanotube, and the patterned fluid reservoirs; while Figure S2 displays the Raman spectra of two representative pristine SWCNTs. The experiment design is similar to the microfluidic setup employed by Liu and co-workers.[17] Oxygen plasma treatment is used to cut the unwanted parts of the SWCNT and open both of its ends. The length of the SWCNT in the device is 20 μm. The diameter of the SWCNTs (1.5 ± 0.4 nm, Figure S3) is comparable to biological nanopores.[19,25] A polydimethylsiloxane (PDMS) polymer block with microfluidic channels is then placed on top of the poly(methyl methacrylate) (PMMA) layer to keep the two reservoirs completely separated and sealed apart while delivering liquid to each one individually. We examine ion conduction through these SWCNT devices by studying the effect of electrolyte concentration and composition on ionic conductance and reverse potential. The reversal potential refers to the bias necessary to suppress ionic flux and yield no ionic current.[1,26] Each experiment is performed on multiple devices, and the relative standard deviation (RSD %) associated with the data was estimated from three repetitions of conductance−concentration and reversal potential−concentration curves in KCl solution. The typical RSD % for conductance−concentration and reversal potential−concentration curves for a representative device are ∼7% and ∼3%, respectively (see Figure S4).

We also prepared a series of control experiments to be run in parallel to the ion transport experiments. They have the same architecture but lack the SWCNT channel. Control devices prepared with the same level of oxygen plasma treatment (10 s) as the ones described above resulted in completely isolated reservoirs and therefore no ionic current. We found that longer (30 s) oxygen plasma treatment resulted in cracks in the PMMA surface. Thus, after deposition of the PDMS block a complete seal is not attained allowing ionic transport across the two reservoirs (Figure S1b).

Ion Selectivity. Because the ring of carboxylates at the entryway of the SWCNTs provides a similar electrostatic environment to the rings or clusters of charges found at the opening of protein ion channels, we can characterize their ion transport using well-established biological methods. These charges provide selectivity between anions and cations in protein ion channels.[24] These channels are selective toward the ions carrying the opposite charge to that of the channel entrance region. Therefore, if carboxylates that terminate the SWCNTs are similarly effective, then their channels should preferentially transport cations. Indeed, examining the relationship between ionic conductance and monovalent equivalent concentration of salt for a series of electrolytes with varying ion sizes shows that cations are the main charge carriers through SWCNTs (Figure 2a, Device 1). Potassium salts, namely, KCl and $K_3[Fe(CN)_6]$, display comparable conductance values suggesting that the size and mobility of the anion has a negligible effect on the ion transport. However, for cations a significant size-dependent conductance is observed as demonstrated when potassium ions (in KCl) are exchanged for larger tris(bipyridine)ruthenium(II) ions in $[Ru(bpy)_3]Cl_2$. For comparison, the latter two salts in control devices display a smaller conductance divergence (see Figure S5).

We study the permeability of cations versus anions in SWCNTs by using a concentration differential between the two electrolyte reservoirs. We fix the electrolyte concentration in reservoir 1 at 10 mM while gradually increasing the salt concentration of reservoir 2 from 10 mM to 1.0 M. The reversal potentials are always positive on the more dilute side, which is consistent with the cation selectivity of these channels. The permeability ratio of cations over anions (P_c/P_a) in KCl is 121 ± 5 for the device shown according to the Goldman−Hodgkin−Katz (GHK) formalism (Figure 2b, Device 1).[1,27,28] In comparison, native (with no negative charges at the pore entrance) and succinylated porins (*Rhodobacter capsulatus*, negatively charged pore) and Hemolysins (negatively charged pore) display P_c/P_a in KCl of ∼9, ∼ 23, and ∼9, respectively.[25,29] Similarly, the selectivity of cation/anion in

DOI: 10.1021/acs.nanolett.6b04967
Nano Lett. 2017, 17, 1204−1211

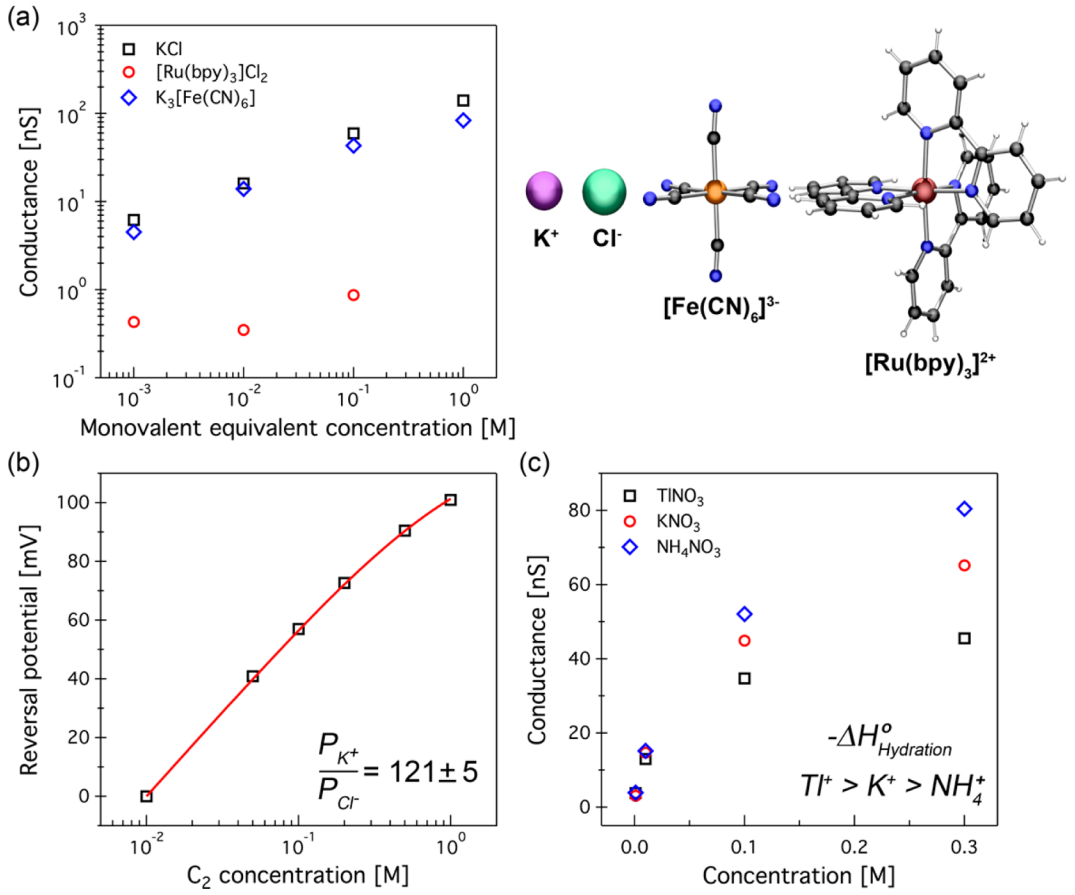

Figure 2. Ion permeability through SWCNTs (Device 1). (a) Effect of ion size on conductance. Ionic conductance is plotted as a function of monovalent equivalent concentration of electrolytes with varying ion sizes. Comparing the conductance−concentration curves of KCl (black squares), $K_3[Fe(CN)_6]$ (blue diamonds), and $[Ru(bpy)_3]Cl_2$ (red circles) suggests that cations are the major charge carriers through carbon nanotubes. (b) Reversal potential (E_{rev}) as a function of KCl concentration in reservoir 2. Concentration of KCl in reservoir 1 was fixed at 10 mM, while in reservoir 2 [KCl] was varied between 10 mM and 1.0 M. E_{rev} was always positive on the more dilute side confirming the cation selectivity of these channels. The solid line is the best fit of data according to the GHK equation yielding a permeability ratio of 121 ± 5 for cations over anions in KCl. (c) Effect of cation enthalpy of hydration. Conductance comparison among KNO_3 (red circles), NH_4NO_3 (blue diamonds), and $TlNO_3$ (black squares) electrolytes with various concentrations at a pH of ∼6.0. Cations with lower absolute value of enthalpy of hydration exhibit higher conductance.

leakage or control devices (without a SWCNT) is poor and displays P_c/P_a of ∼5 (Figure S6).

We compare the conductance of KNO_3, NH_4NO_3, and $TlNO_3$ electrolytes at various concentrations and find that these SWCNTs have a remarkable ability to differentiate K^+ from similar cations, Tl^+ and NH_4^+. NH_4^+ (Tl^+) only differ from K^+ by ∼11% (5%), 0% (1%), and 0% (2%) in crystal radii, hydrated radii, and bulk mobility, respectively.[30,31] Therefore, one would naively expect that K^+, NH_4^+, and Tl^+ would possess similar permeation properties (see Figure S7, Table S1), which is not the case. For all concentrations studied, the conductance decreases with hydration enthalpy[32] of the associated cations in bulk. Thus, the cations with more loosely held water molecules in their hydration shell exhibit higher conductance (NH_4^+ > K^+ > Tl^+, Figure 2c Device 1). This observation reflects the energetic penalty to change the ions' hydration state while traversing a confined hydrophobic nanopore, a feature that is predicted by molecular dynamics simulations.[33,34] A similar selectivity is seen in biological ion selective channels. For example, CaK channels are highly selective for K^+ over the smaller Na^+ and are able to distinguish between K^+ and its analogues, Tl^+, Rb^+, and NH_4^+.[35,36]

Location and Nature of Pore Charges. To confirm that the negative surface charges affecting the ion transport through SWCNTs are localized at the nanotube entrance and not along its core, we study the effects of surface charge modification on the reversal potential using the methodology of Scruggs and co-workers.[26] First, we measure the reversal potential as we decrease the concentration of KCl solutions.[37] The ratio between the concentrations of the two reservoirs, however, is fixed at 2:1 to keep the contribution of the diffusion potential (proportional to the concentration gradient) constant with respect to the reversal potential. Figure 3a for Device 1 demonstrates that as KCl concentration decreases from 1000 to 0.1 mM (in the more dilute reservoir) the reversal potential sharply decreases (in absolute value) until it eventually plateaus at concentrations below 1.0 mM. We expect this behavior because of the presence of fixed charges on the two ends of the nanotube redistributing the ions and establishing two electrostatic potentials, known as Donnan potentials,[38,39] that contribute to the reversal potential.[37] The effects of surface charges and the resulting Donnan potentials are the largest at low ionic strengths when the charge screening effect of the electrolyte is small.

DOI: 10.1021/acs.nanolett.6b04967
Nano Lett. 2017, 17, 1204−1211

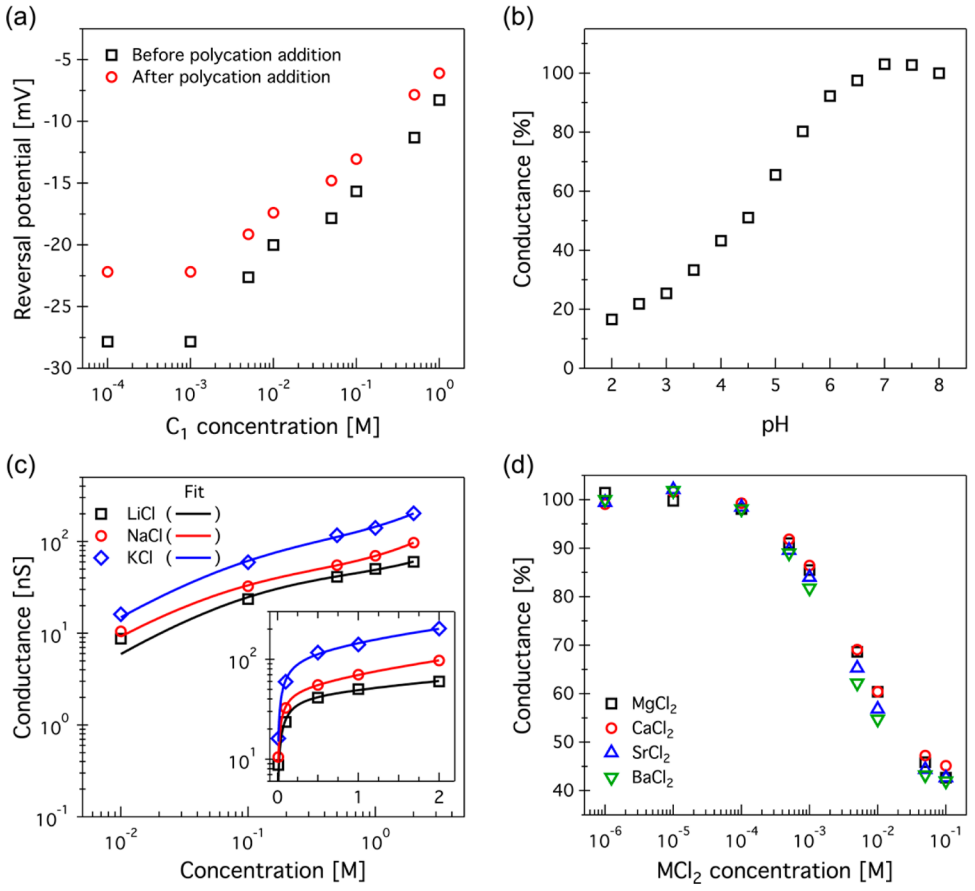

Figure 3. Probing the electrostatic mechanism and conduction across SWCNTs (Device 1). (a) Reversal potential modulation of the surface potential was accomplished using electrolyte screening or electrostatic adsorption of polycations. The KCl concentration in reservoir 2 was always equal to 2 times the concentration of KCl in reservoir 1. Reversal potential as a function of KCl concentration in reservoir 1 before (black squares) and after (red circles) addition of a small amount of polycation to reservoir 1. (b) Conductance variation, with respect to the solution with pH = 7.0. Data recorded as we symmetrically reduced the pH of 100 mM KCl solutions from 8.0 to 2.0. An approximate pK_a of ∼5 is observed for the channel functional groups. (c) Ionic conductance dependence on concentration of LiCl (black squares), NaCl (red circles), and KCl (blue diamonds) electrolytes in the low to medium concentration range. Solid lines are the best fit of data according to the electrostatic model described in the main text. Inset: same ionic conductance data as in (c) plotted on a linear concentration axis. (d) Effect of cation valency on conductance. Conductance modulation with respect to 200 mM KCl divalent-free solutions as divalent salt is added. $MgCl_2$ (black squares), $CaCl_2$ (red circles), $SrCl_2$ (blue triangles), and $BaCl_2$ (green triangles).

Furthermore, a smaller absolute reverse potential is expected if these fixed charges are screened or counterbalanced. This hypothesis was tested by using cationic and anionic polymers since these would not be carried through the nanotube but would provide a means to screen these charges. For these measurements a small amount of a polycation solution of poly(dimethylamine-*co*-epichlorohydrin-*co*-ethylenediamine) (M_W ≈ 75,000, concentration of 20 μg/mL) was added to reservoir 1 (Figure 3a, Device 1). Since the positively charged polymer chains are too large to pass through the nanotube, they remain at the SWCNT entrance. However, their electrostatic adsorption onto the negatively charged pore mouth reverses the charge and modulates the Donnan potential on that end of the SWCNT. The overall effect is a reduced absolute reverse potential as seen in Figure 3a (red circles). Control experiments on the devices with intentional leakage pathways provide further evidence of this electrostatic absorption. Since conduction is not mediated through a charged pore entrance, as in the SWCNT devices, the reversal potential remains the same whether the polycation is present or not in reservoir 1 (see Figure S8). At low ionic strengths (≤1.0 mM), the addition of polycations causes a considerable upward shift in reversal potential; however, the effect is progressively smaller with increasing ionic strength and screening of the surface charges (Figure 3a, red circles). In contrast, the conductance is unaffected when ionic current is measured on SWCNT and control devices with intentional leakage pathways using a polyanion, poly(sodium 4-styrenesulfonate) (M_W ≈ 70,000, concentration of 20 μg/mL). This eliminates the possibility of nonspecific adsorption of polymers onto the nanotube entrance (see Figure S9).

Study of conductance as a function of pH provides evidence on the chemical nature of surface charges. The recorded conductance of 100 mM KCl (with 2.0 mM of buffering agent) in the pH range of 2.0−8.0 produces a simple titration curve (Figure 3b, Device 1). The data shows an approximate pK_a of ∼5 consistent with carboxylate groups at the cut ends of CNT in aqueous solutions.[21] The strong pH dependence of channel conductance highlights the significance of the protonation state of carboxyl groups at CNT ends and the local electric potentials created by these groups. In contrast, control experiments show only a weak pH dependence likely the result of protonation of silanol, hydroxyl, and other pH-related groups, formed on the surface of PDMS and PMMA by oxygen plasma treatment (see

DOI: 10.1021/acs.nanolett.6b04967
Nano Lett. 2017, 17, 1204−1211

Figure S10). Others have also seen a reduction in ionic current through individuals or large collections of carbon nanotubes at low pH values.[17,40,41]

Conductance Dependence on Ionic Concentration, an Electrostatic Mechanism. Now that we have established the role of the carboxylates at the SWCNT entrance, we can construct a model based on this electrostatic potential to understand the ionic conduction across SWCNTs. Previous studies have shown that the conductance (G) of narrow SWCNTs in symmetrical KCl solutions follows a power law dependence as a function of concentration (C), $G(C) \propto C^a$; where the exponent (a) has been found to be ~0.4.[17,42] The authors attributed the cation selectivity and transport to both the negative charges distributed along and at the entrance of the SWCNT. The data we collected follows a power law dependence approximating $C^{0.5}$ (Figure S13b, Table S2). This is similar to the conductance−concentration profile of many biological pore-forming proteins (e.g., certain potassium channels,[43] hemolysins,[29] and modified porins[25,44]). In these, the ion transport experiences a local electrostatic potential, which at the channel entrance has a power law dependence of ~0.5; in contrast ion diffusion through noncharged native porins follows an almost linear dependence (green triangles Figure S13c−d). We would expect this behavior too if the local concentration of current-carrying counterions near the pore mouth is increased through electrostatic interactions. We do not see any appreciable effect from charges along the wall of the SWCNT. At low ionic strengths, the surface potential is largest, and it raises the counterion concentration near the channel entrance.[45] As the ionic strength is increased, the surface potential is screened and the local concentration of counterions is buffered. Therefore, at low ionic strengths, conductance is higher than expected, and it rapidly increases with concentration, while it only slightly varies near the maximum conductance of the channel.[22]

Figure 3c shows plots of SWCNTs conductance with LiCl, NaCl, or KCl electrolytes over the range of 10 mM to 2.0 M, in a log−log plot for Device 1 (Figure 3c inset displays the conductance−concentration data in a log−linear form for comparison). Although the observed conductance values depend on the electrolyte type, the shapes of the conductance−concentration curves are identical for all three salts. For protein ion channels, a simple electrostatic model based on the Gouy−Chapman theory of the electrical double layer is used to find the conductance as a function of concentration by calculating the local concentration of counterions near the channel entrance as a function of bulk concentration and surface potential at the channel entrance.[22,45] The channel conductance is then determined by the local concentration of permeant ions at the channel mouth.

In this model, ions in the bulk phase see the negatively charged groups at the channel entrance as an effective point charge, q, which establishes a negative surface potential, Φ. This local potential gives rise to the buildup of an electrical double layer, or a counterion cloud at the channel mouth, which ultimately leads to the channels' overall selectivity, cation over anion and multivalent over monovalent.[25]

The surface potential dependence on bulk ionic strength and pore radius (r) can be estimated from the Gouy−Chapman theory as follows:

$$\Phi = \frac{q}{4\pi\varepsilon_0\varepsilon r}\cdot e^{-r/\lambda_D} \tag{1}$$

where the Debye length (λ_D) is a parameter that determines how far the electrostatic potentials are extended in the solution and depends on the ionic strength of the electrolyte; ε_0 and ε are the absolute dielectric constant of free space and the relative dielectric constant of water, respectively. When the channel radius is smaller than λ_D, the concentration of cations near the channel mouth is larger than that in the bulk. This elevated concentration at the pore entrance (C^+_{local}) can be obtained from the Boltzmann distribution:

$$C^+_{local} = C^+_{bulk}\cdot e^{-z\Phi F/RT} \tag{2}$$

where C^+_{bulk} is the ion's bulk concentration, z is the charge on the ion, and R, T, and F have their standard thermodynamic significance. Hence, the total conductance $(G(C))$ across the SWCNT can now be written as the product of the molar conductance (G_{molar}) and the local cation concentration:

$$G(C) = G_{molar}\cdot C^+_{local} \tag{3}$$

When we apply this model to the conductance of SWCNT across >2 orders of magnitude of ion concentration we obtain the fits displayed in Figure 3c. Free refinement of the data produces: $14.8 < G_{molar} < 67.9$ nS/M, $0.38 < r < 0.52$ nm, and $-2.9 < q < -2.2\ e^-$ as displayed in Figure 3c. Alternatively, fixing the SWCNT radius to a more realistic diameter (1.5 nm, see Supporting Information Figure S3), we obtain $28.9 < G_{molar} < 93.6$ nS/M and $-5.0 < q < -4.4\ e^-$, which also provides a more intuitive value for the effective q (see Supporting Information Figure S13a and Table S2).

We find that the conductance is strongly dependent on the valence of the screening ion but not on its type.[24] Again, this points to the importance of the carboxylates at the opening of the SWCNTs for controlling the ion transport. We measure the conductance of 200 mM KCl solution, at varying concentrations of added $MgCl_2$, $CaCl_2$, $SrCl_2$, or $BaCl_2$. Figure 3d shows the normalized conductance of Device 1 with respect to the conductance of 200 mM KCl divalent-free solutions as a function of the divalent salt concentration. Upon the addition of divalent cations, conductance not only does not rise, as in control experiments (see Figure S11), it also sharply declines and eventually levels off at some nonzero value. This reduction in ionic conductance with the addition of divalent cations results from the electrostatic screening of surface charges; divalent cations screen the surface charges to a much greater extent than the similar concentration of monovalent cations (see eq 2).[22,24] The reduction of conductance is also independent of the nature of the divalent species (Figure 3d), indicating that divalent cations neither block the SWCNT pore nor bind to the carboxyl groups but simply screen the surface charges at the pore mouth.[24,46] These results further support the proposed electrostatic mechanism for explaining ion conduction through narrow SWCNTs. Again, protein ion channels with fixed charges at the mouth, such as CaK, produce similar results and conclusions under similar experimental conditions.[47]

Multi-Ion Channel Behavior. Certain protein channels can accommodate multiple ions in a queue within their permeation pathway.[1] The mutual repulsions between ions enforce a correlation in ion motions and prevent them from passing one another, even if they are small enough in size. It is often observed experimentally that the conductance of multi-ion pores reaches a maximum value and then starts a descending phase as the concentration of permeate ion is raised to

DOI: 10.1021/acs.nanolett.6b04967
Nano Lett. 2017, 17, 1204−1211

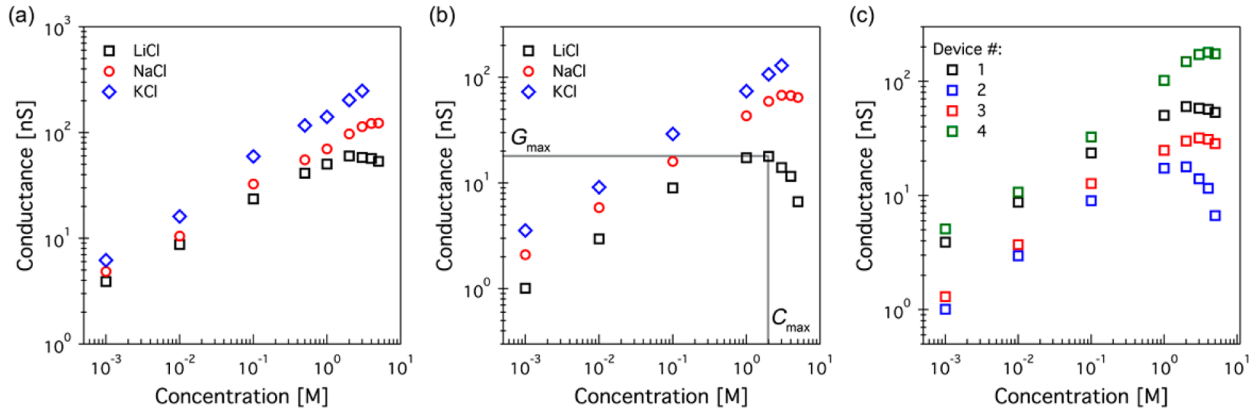

Figure 4. Conductance reduction at high ion concentrations. Ionic conductance dependence of (a) Device 1 and (b) Device 2 on the concentration of LiCl (black squares), NaCl (red circles), and KCl (blue diamonds) electrolytes in the low to high concentration range. (c) Ionic conductance dependence on LiCl concentration in four CNT devices with different conductivity levels.

sufficiently high levels on both sides of the membrane.[48,49] One model used to explain the conductance reduction in biological channels proposes that ions need vacancies inside the channel to move into in order to maintain the flux.[50] At high ion concentrations the channel is saturated with ions, and as one ion exits the pore into the solution and leaves behind a vacancy for its following ions to move into, another ion from the same solution fills the pore. Therefore, in channels with multi-ion occupancy, such as CaK, the conductance inhibition at sufficiently high ion concentrations is typically observed.[51]

Conductance−concentration profiles of the SWCNTs also exhibit a descending phase at high concentrations (≥2.0 M), which can be explained through the same multi-ion conduction mechanism. Figure 4 [a (Device 1), b (Device 2)] shows the changes in ionic conductance as the concentration of LiCl, NaCl, or KCl electrolyte is varied over a large range in each of the two SWCNT devices. Figure 4c compares the LiCl conductance−concentration graphs measured in four different SWCNT devices. In a single device, the electrolyte with the lower conductivity level always appears to exhibit a conductance maximum (G_{max}) at a lower concentration (C_{max}), see Figure 4a,b. A similar relationship between G_{max} and C_{max} is observed for one electrolyte type across different devices (Figure 4c). Additionally, control devices with an intentional leakage pathways display no maximum in conductance as concentration is increased (Figure S12), which confirm that this multi-ion channel behavior is unique to the ion transport across SWCNT.

The concerted movement of ions along narrow CNTs, in a single-file fashion enforced by mutual repulsions, has been seen in MD simulation studies.[33,52] It is suggested that this type of ion movement is not exclusive to biological channels and is most likely related to the transport of hydrated ions through hydrophobic confined nanopores.[52] Moreover, MD simulations suggest that ions encounter free energy barriers when entering/exiting narrow CNTs.[33,34] The presence of these concentration-independent steps along the permeation pathway explains the saturation kinetics in these nanotubes.[1,53] The multi-ion conduction mechanism can also justify the observed relationship between G_{max} and C_{max}. Conductance inhibition occurs when the channel is saturated. Hence, when the ion concentration is high enough and the entry rate exceeds the internal transport rate, ions exiting at one side will tend to have ion reentry from the same side; in addition, less conductive channels/electrolytes often reach saturation at lower and more experimentally accessible concentrations.[54] For instance, a conductance maximum is not observed in CaK channels up to 2.0 M of K^+; however, it is detected when less conductive Rb^+ is used instead.[36,51]

Conclusions. This study unravels the ion transport mechanisms of small diameter single-walled carbon nanotubes and finds that they are essentially mimics of ion channels found in nature. The diameters of both the SWCNT channels and the biological channels are in a length-scale where the behavior of fluids and the factors governing the transport begin to deviate from continuum descriptions of fluidic dynamics because the molecular nature and complex interplay among channel, water, and ions become significant.[55−57] We find that the ion charge, size, and hydration enthalpy are the main factors that dictate the conductance of a given ion through SWCNTs. The SWCNT has electrostatic potentials, arising from deprotonated carboxyl groups at the nanopore entrance, that are critical in the resulting ion selectivity, gating, and permeation through the SWCNTs. We model our experimental results from the one that has been developed for protein ion channels. This model is built on a simplified version of the Gouy−Chapman theory of the electrical double layer. Moreover, the descending conductance phase of our narrow CNT devices at high ion concentration originates from ion−ion interactions inside the nanotube, forcing a single file conductance of ions.

SWCNTs hold great potential for nanofluidic-based technology due to their structural precision, simplicity, uniqueness, and compatibilities with current nanofabrication techniques. The functional groups at SWCNT openings provide a valuable point of diversification to control the ion/molecule flow in sensing, gating, and filtering applications.[58−60] Above all, ion transport through small diameter SWCNTs share many general similarities with their biological counterparts, which make them promising candidates for the development of artificial biomimetic nanopores.

■ ASSOCIATED CONTENT

Supporting Information

The Supporting Information is available free of charge on the ACS Publications website at DOI: 10.1021/acs.nanolett.6b04967.

Device fabrication and characterization, Raman spectroscopy, atomic force microscopy, ionic conductance and

DOI: 10.1021/acs.nanolett.6b04967
Nano Lett. 2017, 17, 1204−1211

reversal potential measurements of non-SWCNT devices (control experiments), and fitting of literature data to modified Gouy−Chapman model described herein (PDF)

AUTHOR INFORMATION

Corresponding Authors

*E-mail: shepard@ee.columbia.edu.
*E-mail: cn37@columbia.edu.
*E-mail: rh2780@columbia.edu.

ORCID

Colin Nuckolls: 0000-0002-0384-5493

Notes

The authors declare no competing financial interest.

ACKNOWLEDGMENTS

C.N. thanks Sheldon and Dorothea Buckler for their generous support. R.H.S. acknowledges the support from the Columbia Nano Initiative Postdoctoral Fellowship. Research reported in this publication was supported by the National Institute of General Medical Sciences of the National Institutes of Health under Award Number R01GM107417. The content is solely the responsibility of the authors and does not necessarily represent the official views of the National Institutes of Health.

REFERENCES

(1) Hille, B. *Ion Channels of Excitable Membranes*, 3rd ed.; Sinauer: Sunderland, MA, 2001; p xviii.
(2) Wood, C.; Williams, C.; Waldron, G. J. *Drug Discovery Today* **2004**, *9* (10), 434−441.
(3) Dworakowska, B.; Dolowy, K. *Acta Biochim. Polym.* **2000**, *47* (3), 685−703.
(4) Proks, P.; Lippiat, J. D. *Curr. Pharm. Des.* **2006**, *12* (4), 485−501.
(5) Kowalczyk, S. W.; Blosser, T. R.; Dekker, C. *Trends Biotechnol.* **2011**, *29* (12), 607−614.
(6) Yameen, B.; Ali, M.; Neumann, R.; Ensinger, W.; Knoll, W.; Azzaroni, O. *Nano Lett.* **2009**, *9* (7), 2788−2793.
(7) Hou, X.; Guo, W.; Xia, F.; Nie, F. Q.; Dong, H.; Tian, Y.; Wen, L.; Wang, L.; Cao, L.; Yang, Y.; Xue, J.; Song, Y.; Wang, Y.; Liu, D.; Jiang, L. *J. Am. Chem. Soc.* **2009**, *131* (22), 7800−5.
(8) Tian, Y.; Hou, X.; Wen, L. P.; Guo, W.; Song, Y. L.; Sun, H. Z.; Wang, Y. G.; Jiang, L.; Zhu, D. B. *Chem. Commun.* **2010**, *46* (10), 1682−1684.
(9) Siwy, Z. S.; Howorka, S. *Chem. Soc. Rev.* **2010**, *39* (3), 1115−1132.
(10) Venkatesan, B. M.; Bashir, R. *Nat. Nanotechnol.* **2011**, *6* (10), 615−624.
(11) Ho, C.; Qiao, R.; Heng, J. B.; Chatterjee, A.; Timp, R. J.; Aluru, N. R.; Timp, G. *Proc. Natl. Acad. Sci. U. S. A.* **2005**, *102* (30), 10445−10450.
(12) Dekker, C. *Nat. Nanotechnol.* **2007**, *2* (4), 209−215.
(13) Hummer, G.; Rasaiah, J. C.; Noworyta, J. P. *Nature* **2001**, *414* (6860), 188−190.
(14) Fornasiero, F.; Bin In, J.; Kim, S.; Park, H. G.; Wang, Y.; Grigoropoulos, C. P.; Noy, A.; Bakajin, O. *Langmuir* **2010**, *26* (18), 14848−14853.
(15) Dalla Bernardina, S.; Paineau, E.; Brubach, J.-B.; Judeinstein, P.; Rouzière, S.; Launois, P.; Roy, P. *J. Am. Chem. Soc.* **2016**, *138* (33), 10437−10443.
(16) Lin, T.; Bajpai, V.; Ji, T.; Dai, L. M. *Aust. J. Chem.* **2003**, *56* (7), 635−651.
(17) Liu, H. T.; He, J.; Tang, J. Y.; Liu, H.; Pang, P.; Cao, D.; Krstic, P.; Joseph, S.; Lindsay, S.; Nuckolls, C. *Science* **2010**, *327* (5961), 64−67.
(18) Liu, L.; Yang, C.; Zhao, K.; Li, J. Y.; Wu, H. C. *Nat. Commun.* **2013**, *4*, 3989.
(19) Jiang, Y. X.; Lee, A.; Chen, J. Y.; Cadene, M.; Chait, B. T.; MacKinnon, R. *Nature* **2002**, *417* (6888), 515−522.
(20) Brelidze, T. I.; Niu, X. W.; Magleby, K. L. *Proc. Natl. Acad. Sci. U. S. A.* **2003**, *100* (15), 9017−9022.
(21) Wong, S. S.; Joselevich, E.; Woolley, A. T.; Cheung, C. L.; Lieber, C. M. *Nature* **1998**, *394* (6688), 52−55.
(22) Dani, J. A. *Biophys. J.* **1986**, *49* (3), 607−618.
(23) Jordan, P. C. *Biophys. J.* **1987**, *51* (2), 297−311.
(24) Green, W. N.; Andersen, O. S. *Annu. Rev. Physiol.* **1991**, *53*, 341−359.
(25) Welte, W.; Diederichs, K.; Przybylski, M.; Glocker, M. O.; Benz, R.; Breed, J. *Nato Adv. Sci. I. C-Mater.* **1998**, *510*, 239−276.
(26) Scruggs, N. R.; Robertson, J. W. F.; Kasianowicz, J. J.; Migler, K. B. *Nano Lett.* **2009**, *9* (11), 3853−3859.
(27) Goldman, D. E. *J. Gen. Physiol.* **1944**, *27* (1), 37−60.
(28) Hodgkin, A. L.; Katz, B. *J. Physiol.* **1949**, *108* (1), 37−77.
(29) Benz, R.; Schmid, A.; Wagner, W.; Goebel, W. *Infect. Immun.* **1989**, *57* (3), 887−895.
(30) Nightingale, E. R. *J. Phys. Chem.* **1959**, *63* (9), 1381−1387.
(31) Barry, P. H.; Lynch, J. W. *J. Membr. Biol.* **1991**, *121* (2), 101−117.
(32) Smith, D. W. *J. Chem. Educ.* **1977**, *54* (9), 540−542.
(33) Liu, H. M.; Murad, S.; Jameson, C. J. *J. Chem. Phys.* **2006**, *125* (8), 084713.
(34) Song, C.; Corry, B. *J. Phys. Chem. B* **2009**, *113* (21), 7642−7649.
(35) Blatz, A. L.; Magleby, K. L. *J. Gen. Physiol.* **1984**, *84* (1), 1−23.
(36) Eisenman, G.; Latorre, R.; Miller, C. *Biophys. J.* **1986**, *50* (6), 1025−34.
(37) Schaep, J.; Vandecasteele, C. *J. Membr. Sci.* **2001**, *188* (1), 129−136.
(38) Donnan, F. G. *Chem. Rev.* **1924**, *1* (1), 73−90.
(39) Donnan, F. G. *J. Membr. Sci.* **1995**, *100* (1), 45−55.
(40) Miller, S. A.; Young, V. Y.; Martin, C. R. *J. Am. Chem. Soc.* **2001**, *123* (49), 12335−12342.
(41) Wu, J.; Gerstandt, K.; Zhang, H. B.; Liu, J.; Hinds, B. J. *Nat. Nanotechnol.* **2012**, *7* (2), 133−139.
(42) Pang, P.; He, J.; Park, J. H.; Krstic, P. S.; Lindsay, S. *ACS Nano* **2011**, *5* (9), 7277−7283.
(43) Sakmann, B.; Trube, G. *J. Physiol.* **1984**, *347*, 641.
(44) Trias, J. Q.; Benz, R. *J. Biol. Chem.* **1993**, *268* (9), 6234−6240.
(45) Nelson, A. P.; McQuarrie, D. A. *J. Theor. Biol.* **1975**, *55* (1), 13−27.
(46) Green, W. N.; Weiss, L. B.; Andersen, O. S. *J. Gen. Physiol.* **1987**, *89* (6), 841−872.
(47) MacKinnon, R.; Latorre, R.; Miller, C. *Biochemistry* **1989**, *28* (20), 8092−8099.
(48) Neher, E.; Sandblom, J.; Eisenman, G. *J. Membr. Biol.* **1978**, *40* (2), 97−116.
(49) Urban, B. W.; Hladky, S. B.; Haydon, D. A. *Biochim. Biophys. Acta, Biomembr.* **1980**, *602* (2), 331−354.
(50) Hille, B.; Schwarz, W. *J. Gen. Physiol.* **1978**, *72* (4), 409−442.
(51) Villarroel, A.; Alvarez, O.; Eisenman, G. *Biophys. J.* **1988**, *53*, 259a.
(52) Sumikama, T.; Saito, S.; Ohmine, I. *J. Phys. Chem. B* **2006**, *110* (41), 20671−7.
(53) Hilder, T. A.; Gordon, D.; Chung, S. H. *Biophys. J.* **2010**, *99* (6), 1734−1742.
(54) Lu, Z.; MacKinnon, R. *J. Gen. Physiol.* **1994**, *104* (3), 477−86.
(55) Travis, K. P.; Todd, B. D.; Evans, D. J. *Phys. Rev. E: Stat. Phys., Plasmas, Fluids, Relat. Interdiscip. Top.* **1997**, *55* (4), 4288−4295.
(56) Qiao, R.; Aluru, N. R. *J. Chem. Phys.* **2003**, *118* (10), 4692−4701.
(57) Huang, C. K.; Choi, P. Y. K.; Nandakumar, K.; Kostiuk, L. W. *J. Chem. Phys.* **2007**, *126* (22), 224702.
(58) Hinds, B. J.; Chopra, N.; Rantell, T.; Andrews, R.; Gavalas, V.; Bachas, L. G. *Science* **2004**, *303* (5654), 62−65.

DOI: 10.1021/acs.nanolett.6b04967
Nano Lett. 2017, 17, 1204−1211

(59) Majumder, M.; Chopra, N.; Hinds, B. J. *J. Am. Chem. Soc.* **2005**, *127* (25), 9062−9070.
(60) Majumder, M.; Zhan, X.; Andrews, R.; Hinds, B. J. *Langmuir* **2007**, *23* (16), 8624−8631.

DOI: 10.1021/acs.nanolett.6b04967
Nano Lett. 2017, 17, 1204−1211